Perturbational Simulation and Experimentation for Calibrated RF Cavity Measurements

Alex Pizzuto

Loyola University Chicago
Argonne National Laboratory
apizzuto@luc.edu

August 12, 2016

Abstract

Field strength measurements for determination of the R/Q of various modes in RF cavities rely on perturbational techniques with analytically approximated perturbing objects. Simulations and analytical approximations were compared to measured results on cavities with calculable fields for a repository of perturbing objects to perform calibrated measurements. Categorized perturbing objects were then used to perform calibrated measurements of the accelerating mode of 86-cell $\frac{2\pi}{3}$ 2.856 GHz cavities that had been straightened after deformations due to gravitational effects as well as higher order modes (HOMs) of the 352 MHz Advanced Photon Source storage ring cavities.

I. Introduction

Throughout their installation at the Advanced Photon Source (APS) at Argonne, various structures underwent unpredicted gravitational deformations. During various shutdowns, these cavities are pulled from the linear accelerator to undergo straightening and tuning. However, this process may result in a shifting of electrical center as well as offset phase advance in certain cells. These imperfections can cause kicks from HOMs. In order to properly understand the functionality of the cavities in the accelerator, we seek to categorize the modes with their corresponding R/Q, a measure of the cavity shunt impedance divided by the loaded Q of the cavity to provide a performance parameter completely dependent on geometrical factors.

In addition, various problematic longitudinal modes have been witnessed in the 352 MHz cavities in the storage ring. Coupling to longitudinal HOMs leads to increased energy spread and eventual beam loss from receiving energy in the non-restoring sections of the RF voltage curve. In order to better quantify the magnitude of the effects from these HOMs, each mode needs to be associated with a R/Q, in order to determine what feedback systems need to be put into place. These R/Q values are cross-referenced with simulation results from CST Microwave Studio.

In order to make these measurements, classification of the form factors of perturbing objects (beads) is necessary and allows for calibrated field measurements on any future occasion.

II. Theoretical Background

Given a resonant mode of a cavity, the resonant frequency, ω_0, will shift when a perturbing object is introduced to the cavity. The change in frequency was first solved analytically by solving Maxwell's First and Second Equations in the perturbed and unperturbed cavity in [1]. If we denote the local absolute permittivity and permeability of the perturbing object as $\Delta\epsilon$ and $\Delta\mu$, respectively, then it can be shown that the shift in resonant frequency is given by

$$\frac{\Delta\omega}{\omega_0} = -\frac{\int_V (\Delta\epsilon \vec{E} \cdot \vec{E}_0^* + \Delta\mu \vec{H} \cdot \vec{H}_0^*) \cdot dV}{4U} \quad (1)$$

where U is the stored energy in the cavity. If the numerator is known for a certain geometry, then this reduces to

$$\frac{\Delta\omega}{\omega_0} = \frac{1}{U}\left(F_1 E_{\parallel}^2 + F_2 E_{\perp}^2 + F_3 H_{\parallel}^2 + F_4 H_{\perp}^2\right) \quad (2)$$

where the F_i are electric and magnetic form factors of the certain perturbing objects, or beads. In principle, if the fields of a cavity are known, then by measurement of the frequency shift of a mode in the cavity, one can determine the form factors for a certain bead either by introducing the bead into regions where certain components of the field are zero, or by perturbing different fields and solving a system of linear equations.

In practice, in order to compute the magnitude of the field at enough locations to determine field patterns with precision, frequency shift is too imprecise a measurement. Instead, one can indirectly measure the frequency shift by measuring the phase shift of the S_{21} transmission coefficient from the two dimensional scattering matrix, so long as we remain on the linear regime of the curve, we can approximate

$$\frac{\Delta\omega}{\omega_0} \approx \frac{1}{2Q}\tan\left(\Delta\phi_{21}\right).$$

Then, if we recognize the R/Q is the square of the accelerating voltage normalized by the stored energy in the cavity divided by the angular frequency, then we have

$$\frac{R}{Q} = \frac{1}{2\pi\epsilon_0}\left(\int dz\sqrt{\frac{\tan\Delta\phi}{2Q_L}\frac{1}{F_1}}\right)^2,$$

thus by measuring the phase shift as a function of longitudinal position in the cavity, a measured value of R/Q is obtained [2].

III. Analytical Approximations

When the integral in equation 1 is known, the form factors of the beads are equal to the electric or magnetic polarizability of the object times the permittivity or permeability (respectively) of free space. In the case of the perturbing objects available, this is only exactly solvable with a metallic or dielectric (DE) sphere. However, with cylindrical beads, approximations are made by treating the cylinders as prolate or oblate spheroids dependent on the aspect ratio of the bead.

In the case of a sphere, where we substitute ξ as the absolute permittivity and permeability of the object, then we have the form factor for the magnitude of either the electric or magnetic field as

$$F = -\pi a^3 \frac{\xi - 1}{\xi + 2}$$

where a is the radius of the sphere [3]. While the sphere is exactly solvable, its isotropic nature does not allow one to separate the components of the fields. However, if we treat a cylinder as a prolate spheroid (the solid generated by rotation of an ellipse around its major axis) with major axis $l/2$ and minor axis a, then we obtain form factors depending on whether the field is transverse or longitudinal. For example, in the case of a conducting bead in a perturbed field originally parallel or perpendicular to the major axis, the form factors are given by

$$F_1 = -\frac{\pi L^3 \epsilon_0 \left(1 - \frac{4a^2}{L^2}\right)^{3/2}}{12\left(\log\left(\frac{\sqrt{1-\frac{4a^2}{L^2}}+1}{1-\sqrt{1-\frac{4a^2}{L^2}}}\right) - 2\sqrt{1-\frac{4a^2}{L^2}}\right)}$$

$$F_2 = \frac{\pi L^3 \epsilon_0 \left(1 - \frac{4a^2}{L^2}\right)^{3/2}}{6\left(\log\left(\frac{\sqrt{1-\frac{4a^2}{L^2}}+1}{1-\sqrt{1-\frac{4a^2}{L^2}}}\right) - \frac{L^2\sqrt{1-\frac{4a^2}{L^2}}}{2a^2}\right)}.$$

Much work has been done by [3],[4],[5], and [6] to create better approximations using different techniques for different beads. All of our data were compared to these existing models for comparison, but in all models the behavior of longitudinal form factor as opposed to the transverse for cylinders (both hollow needles and solid rods) highlights the capability of being able to isolate certain components of the field.

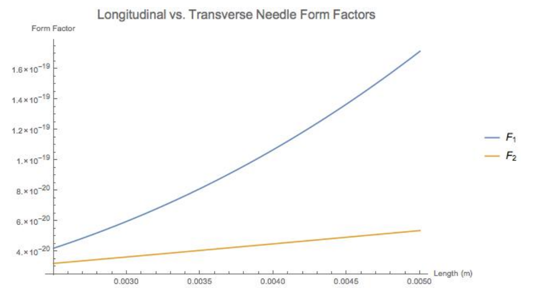

Figure 1: *Approximations for longitudinal and transverse electric field form factors*

IV. Simulation Methods

While the analytical approximations provide a good starting point for bead behavior, and allow for relative measurements, in order to measure precisely, more data is needed that truly fits measured results. In order for the equation 1 to hold, the perturbing object must be small compared to the size of the wavelength of the signal. In our case, calibrated measurements were desired for an S-Band (2.856 GHz) travelling wave structure and structures in lower frequency parts of the UHF regime (352 MHZ fundamental standing wave structure). Both of our cavities exhibit cylindrical symmetry, allowing for precise simulations in Superfish, which were also compared to simulations performed in CST Microwave Studio on a 1.7 GHz pillbox cavity and 2.8 GHz coupled cavity. Simulations were performed for metallic spheres and needles, as well as for both metallic and dielectric rods. These simulations were used to determine which analytical solutions could be used if measured calibrated data did not exist for a bead or if simulation was not available in the future.

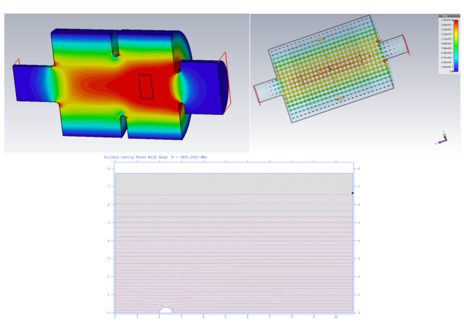

Figure 2: *Microwave Studio Simulations (top) and Superfish simulation (bottom)*

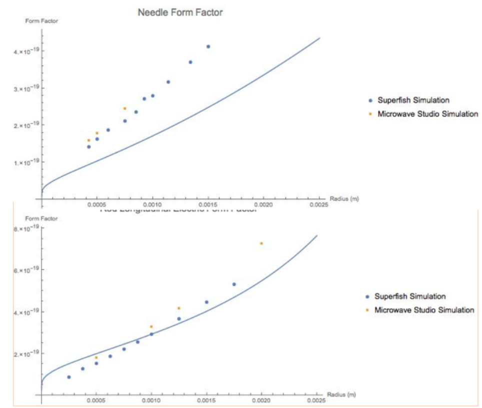

Figure 3: *Comparison of Needle and Rod simulation results*

V. Experimental Results

In order to find values for the form factors of different beads, calculable fields must be perturbed. This requires coupling with cavities in such a way to ensure that the proper modes are excited as well as being sure that one is measuring the fields in the proper transverse position, as it is not always the case that the electrical center maps directly onto the mechanical center of the cavity. For testing purposes, two different cavities, a 1.7 GHz pillbox cavity and a 2.8 GHz coupled cavity, were used.

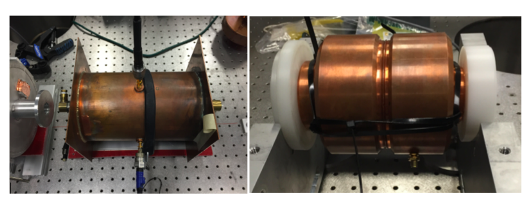

Figure 4: *Cavities used for calibration measurements*

The methodology for locating calculable fields in the pillbox cavity first entailed coupling with the probes to ensure that some

modes were excited.
Maximum coupling for Transverse Electric (TE) or Transverse Magnetic (TM) modes led to minimal coupling with the other. Fundamental TE and TM modes were simulated, and bead-pulls were performed with both maximally coupled modes to determine which probe orientation resulted in the excitation of which modes, by comparison of field flatness. Once resonances

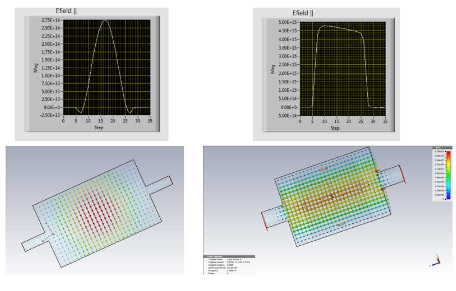

Figure 5: *TE and TM determination*

were visible from the log plot of the S11 reflection coefficient on the precision network analyzer (PNA), bead pulls were performed with dielectric rods (only sensitive to the electric field, and mainly to the longitudinal component), to have a cursory relative mapping of the longitudinal electric field. Though calibration is easiest in modes with on axis longitudinal fields, HOMs with zero field on axis were searched for in order to find electrical center.

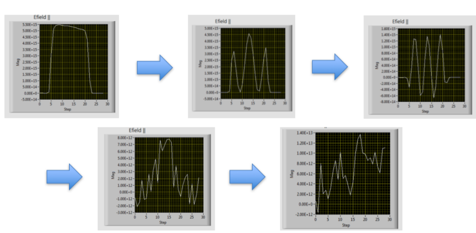

Figure 6: *Bead-Pulls at different frequencies in Pillbox to locate modes with zero on-axis field*

When modes with small magnitude fields at mechanical center were located, their frequencies were cross referenced with simulation results to locate the dipole mode. Once the dipole mode was discovered, at a frequency of 2.747 GHz, relative field strength measurements were taken in 21 transverse locations for 2 different longitudinal coordinates, in order to map the mode transversely and determine the linear electrical center.

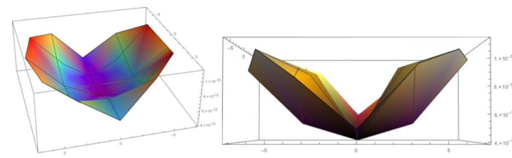

Figure 7: *Mapping of relative field strength of Dipole Mode (left) and $z = 0$, $x = 0$ orientation to show field patterns at small radii (right)*

i. Mode Identification and Exploitation

With the location of electrical center and mode identification from bead-pulls at different resonances, we turned to specific modes to calibrate different form factors for the same beads in calculable fields for the beads listed below.

Table 1: *Beads used for measurement in calculable fields*

Bead	Length (mm)	Radius (mm)
Rod 1	4	0.5
Rod 2	5	1
Rod 3	5	1.25
Rod 4	5	2
Needle 1	5	0.425
Needle 2	5	0.5
Needle 3	5	0.75
DE Rod 1	5	1.5
DE Rod 2	5	2
DE Rod 3	5	2.5
Sphere	N/A	2.35

Each bead has 4 associated form factors for the longitudinal and transverse electric and magnetic field components. By exciting modes that have only one of these components on axis, it is possible to measure the corresponding form factor for each bead. This was done for all components sans the longitudinal magnetic field, as we were not investigating effects due to a longitudinal magnetic field. DE beads only have form factors for the electric field components, as they do not affect the magnetic fields. However, the permittivity of the dielectric beads was unknown, but simulations were performed to place a rough estimate on the magnitude of the permittivity of the beads.

i.1 Longitudinal Electric Field Form Factor

In order to isolate the longitudinal electric field form factor for the beads, we excited the TM_{010} mode of the cavity. In a pillbox cavity, the fields found by setting $B_z = 0$ and solving Maxwell's Equations result in the following field components

$$E_z(\vec{r}) = E_0 J_0(\frac{r}{r_0}) \cos(kz - \omega t)$$
$$B_\phi(\vec{r}) = B_0 J_0'(\frac{r}{r_0}) \sin(kz - \omega t).$$

Thus, E_z will take a maximum on the longitudinal axis, whereas B_ϕ is identically zero on axis.

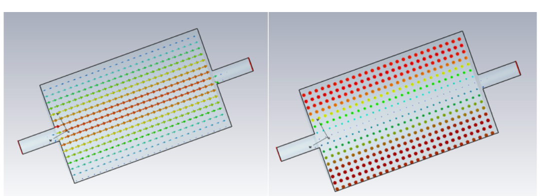

Figure 8: *E-field (left) and H-field (right) for F_1*

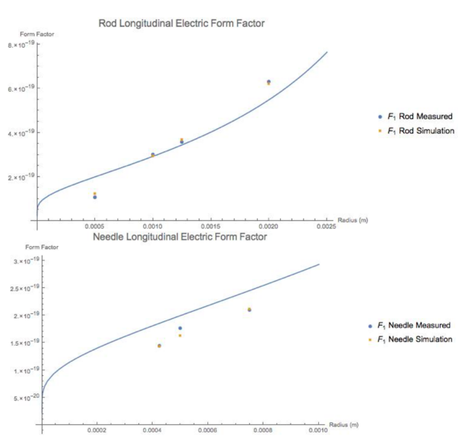

Table 2: *Longitudinal Electric Field Form Factor. All Form Factor values given are $\cdot 10^{-19}$*

Bead	Measured F_1	Simulated F_1	Error
Rod 1	1.079	1.20	9.78%
Rod 2	3.0123	2.90	3.70%
Rod 3	3.567	3.65	2.32%
Rod 4	6.316	6.20	1.85%
Needle 1	1.441	1.42	1.52%
Needle 2	1.768	1.63	8.77%
Needle 3	2.095	2.11	0.75%
DE 1	1.573	1.59	1.17%
DE 2	2.554	2.69	5.16%
DE 3	3.733	3.97	5.88%
Sphere	3.665	3.540	3.70%

These errors are well within the errors shown in [1] and [5], and the contrast between the measured results and available approximations highlight the necessity for calibrated beads to compute reliable R/Q values. However, it is worth noting that these simulations were run on both L-Band and S-Band cavities, and simulation and measured results tend to diverge from the analytical approximations in similar fashions when the size of the wavelength relative to the size of the bead is taken into account.

i.2 Transverse Electric Field Form Factor

The mode used for this form factor, TE_{11} appears in Figure 5. A bead-pull was performed to locate where longitudinally the field took a maximum, and then the beads were placed in that region to measure the response of the resonance.

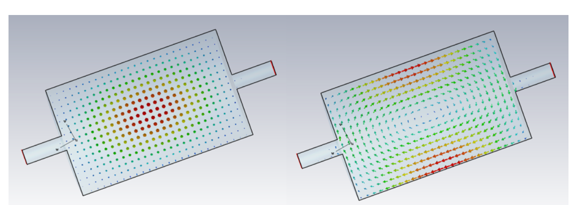

Figure 9: *E-field (left) and H-field (right) for F_2*

The larger errors from the measurements of these form factors are likely a result of the

Table 3: *Transverse Electric Field Form Factor. All Form Factor values given are* $\cdot 10^{-19}$

Bead	Measured F_2	Simulated F_2	Error
Rod 1	0.201	0.156	28.7%
Rod 2	0.802	0.888	9.67%
Rod 3	1.204	1.468	17.9%
Rod 4	3.877	4.425	12.4%
Needle 1	0.134	0.141	4.29%
Needle 2	0.201	0.188	7.16%
Needle 3	0.402	0.459	12.4%
DE 1	1.069	1.337	20.0%
DE 2	2.006	2.472	18.9%
DE 3	3.276	4.026	18.6%
Sphere	3.475	3.659	5.02%

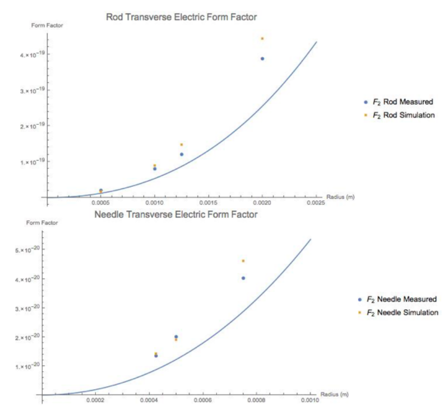

limitations of the PNA, as the magnitude of the frequency and phase shifts are much smaller for cylinders with axis perpendicular to the electric field.

i.3 Transverse Magnetic Field Form Factor

In order to find the transverse magnetic form factors for the beads, the TM_{11} mode was excited. This is a dipole mode that provides kicks to beams if energy is stored in the mode from beam travelling with displacement from electrical center. Centering was extremely important in this case, as with the other modes the electric field did not vary greatly near the axis, but with the dipole mode the R/Q, normalized radially with the first zero of the lowest order Bessel function, increases with the square of the displacement within the radius of the beampipe (where measurement is possible). In general, the magnitude of the frequency shifts from the electric fields is much larger than that due to a magnetic field (for fields of typical respective strength in the cavities), so care was taken to isolate the magnetic field.

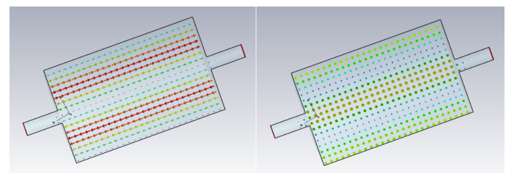

Figure 10: *E-field (left) and H-field (right) for* F_4

For these measurements, DE beads were not used as they do not respond to magnetic fields. However, they do therefor prove useful for locating where the electric field is zero, as the resonant frequency of the cavity should be unperturbed.

Table 4: *Transverse Magnetic Field Form Factor. All Form Factor values given are* $\cdot 10^{-15}$

Bead	Measured F_4	Simulated F_4	Error
Rod 1	-2.193	-2.601	15.7%
Rod 2	-8.655	-9.541	9.28%
Rod 3	-12.97	-15.25	14.9%
Rod 4	-34.62	-33.97	1.90%
Needle 1	-1.454	-1.729	15.9%
Needle 2	-2.885	-3.053	5.5%
Needle 3	-4.316	-6.241	30.8%
Sphere	-25.96	-24.27	7.0%

VI. Calibrated R/Q Measurements

i. Travelling Wave Structures

In order to calculate the R/Q of a multi-cell cavity, one must take into account not only the transit time factor, but also the phase advance per cell.

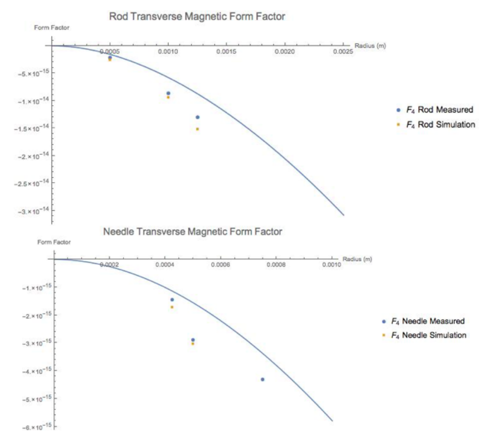

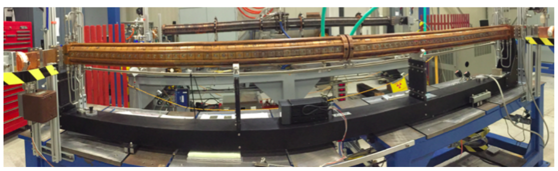

Figure 11: *Structure used for travelling wave R/Q measurement*

In a single cell cavity, the accelerating voltage for a particle travelling at speed βc is given by

$$V_{acc} = \int E_z e^{j\frac{\omega}{\beta c}z} dz$$

However, in a cavity with multiple cells, each cell has a corresponding cell to cell phase advance. This is taken into account as an offset in the argument of the exponential that is incremented upon entry of a new cell. First, a bead-pull was performed that measured the reflection coefficient, and this data was used to obtain the cell to cell phase advance.

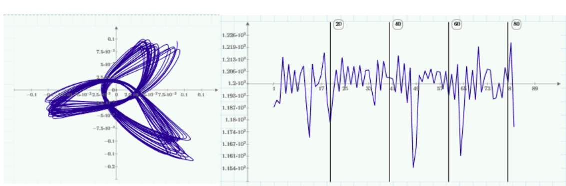

Figure 12: *Sample data for phase advance*

Next, a bead-pull was performed to measure the phase shift in the transmission coefficient to calculate the strength of the field, and these two bead-pulls were combined to calculate the R/Q, where

$$\frac{R}{Q} = \frac{1}{\omega U} |\int E_z e^{j\frac{\omega}{\beta c}z - \phi(z)} dz|^2$$

where $\phi(z)$ is a function of phase advance per cell.

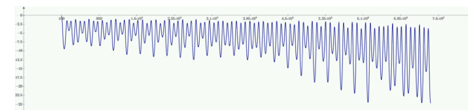

Figure 13: *Sample data for phase shift from perturbation*

As these structures are constant gradient, each cell should provide roughly the same contribution to the R/Q. Taking into account a general shift in the phase of the transmission coefficient, and plotting with energy scaled to reflect only the stored energy in the cavity up the longitudinal coordinate that is our upper bound, we obtain the following plot for the evolution of R/Q in the travelling wave structure.

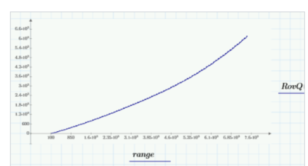

Figure 14: *Evolution of R/Q in the travelling wave cavity*

Using a calibrated bead to measure the R/Q of the travelling wave structure, we obtain a value of 71.125 from our first run and 58.0 from our second, and when compared to the expected prediction of around 70 per cell, we see that our calibrated measuring technique is valid.

After the straightening and tuning process of the cavities used in operations, the desired investigation would be an analysis of the dipole modes of the cavities. However, with operations cavities, there is only the ability to probe the cavity before the input coupler or after the output coupler. In order to properly excite HOMs in a cavity as large as this, probes would need to be placed on individual cells to excite the modes. We attempted to analyze data just from the reflection coefficient in hopes of circumventing the problem of too small a signal being transmitted, but this would just prove that the fields fell off too quickly to obtain a meaningful R/Q for HOMs in a travelling wave structure.

ii. HOM Classification

ii.1 Storage Ring Cavities

Though HOMs on travelling wave structures were not possible to measure with our methodology, cavities in the Storage Ring (SR) at the APS have been under investigation due to their apparent longitudinal HOMs.These HOMs do not provide transverse deflection to beam, but they cause increased energy spread. This not only causes larger buckets and eventual beam loss from leaving buckets, but it also causes dispersion which eventually leads to increased horizontal emittance. These HOMs can be damped with proper feedback systems in place, but for those modes with small R/Q, it is not necessarily obligatory to damp them. To date, only simulations had been done on the longitudinal HOMs, the most problematic of which are pictured below.

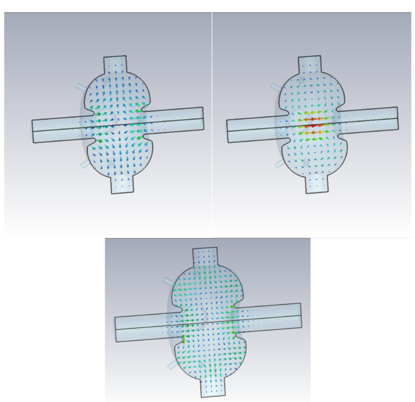

Figure 15: *Longitudinal HOMs of interest in Storage Ring Cavities*

In accordance with practice, a bead-pull was done at the monopole mode to confirm agreement between simulation and measurement.

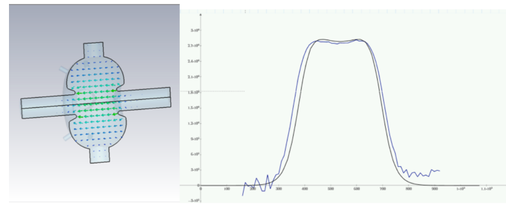

Figure 16: *Simulated and Experimental TM_{010} field strength on axis with experimental field strength in blue*

As we went to investigation of the HOMs, it was noticed that the response of some of these modes was on the order of -.3dB, so measurement was done simultaneously of ϕ_{21} as well as S11. Fits of simulated data were compared to measured data, and these pulls were used to analyze which modes truly pose a threat to energy spread and which resonances are not of interest.

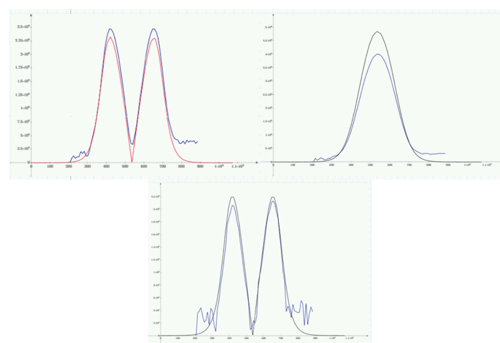

Figure 17: *Fits to longitudinal HOMs*

Table 5: *Longitudinal R/Q values in Storage Ring Cavities*

Frequency (MHz)	Measured	Simulated	Error
352	225.3	226.4	0.5%
535	100	81.8	22.2%
916	8.66	9.1	4.8%
938	8.36	6.6	26.7%

While some modes fit the longitudinal simulations well, this methodology was also useful in determining which resonances that appeared were not problematic. For example, it became clear from pulls which resonances had negligible on axis fields as well as which fit TE mode simulation better.

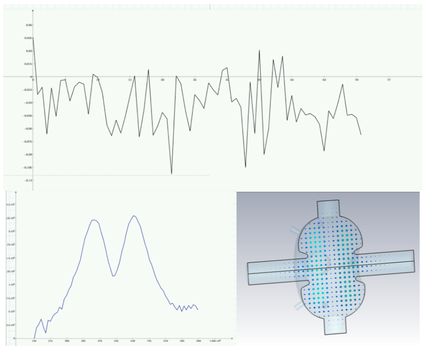

Figure 18: *Resonant mode at 912 MHz (top) showing no on-axis field and mode at 914 MHz (bottom) with corresponding TE mode from simulation*

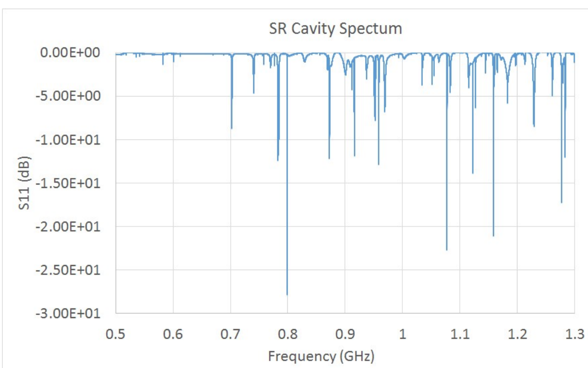

Figure 19: *Early analysis of which resonances are problematic HOMs show that though there are many resonances, not all pose a threat*

VII. Acknowledgements

I would like to thank my mentor on this project, Geoff Waldschmidt, for his unwavering support and guidance. I am also extremely grateful for the assistance of Tim Jonasson, Roy Agner, and Terry Smith in the lab and for the constructive video calls with Massimo dal Forno. In addition, I would like to express my gratitude to the Linda Spentzouris, the Lee Teng Internship, and Illinois Accelerator Institute for making this research possible, and to Eric Prebys for his organizing the internship and lecturing at USPAS.

References

[1] L.C. Maier Jr. and J.C. Slater *Field Strength Measurements in Resonant Cavities.* Journal of Applied Physics 23.68. 1952.

[2] C.M. Bhat *Measurements of Higher Order Modes in 3rd Harmonic RF Cavity at Fermilab* IEEE 1993.

[3] A. Labanc *Electrical axes of TESLA-type cavities.* TESLA Report 2008-01.

[4] H. Hahn and H. Halama *Perturbation Measurement of Transverse R/Q in Iris-Loaded Waveguides.* Microwave Theory and Techniques 16.1. 1968.

[5] P. Matthews et al. *Electromagnetic Field Measurements on a mm-wave Linear Accelerator.* Argonne National Laboratory 1996.

[6] H. Wang and J Guo *Bead-pulling Measurement Principle and Technique Used for the SRF Cavities at JLab.* USPAS 2015.